

Connecting the nuclear EoS to the interplay between fusion and quasifission processes in low-energy nuclear reactions

H. Zheng^{1,2*}, S. Burrello^{2,3}, M. Colonna^{2†}, D. Lacroix⁴, G. Scamps⁵

¹ *School of Physics and Information Technology,
Shaanxi Normal University, Xi'an 710119, China*

² *Laboratori Nazionali del Sud, INFN, I-95123 Catania, Italy*

³ *Departamento de FAMN, Universidad de Sevilla, Apartado 1065, E-41080 Sevilla, Spain*

⁴ *Institut de Physique Nucléaire, IN2P3-CNRS, Université Paris-Sud,
Université Paris-Saclay, F-91406 Orsay Cedex, France and*

⁵ *Center for Computational Sciences, University of Tsukuba, Tsukuba 305-8571, Japan*

Within the Time Dependent Hartree Fock (TDHF) approach, we investigate the impact of several ingredients of the nuclear effective interaction, such as incompressibility, symmetry energy, effective mass, derivative of the Lane potential and surface terms on the exit channel (fusion vs quasifission) observed in the reaction $^{238}\text{U}+^{40}\text{Ca}$, close to the Coulomb barrier. Our results show that all the ingredients listed above contribute to the competition between fusion and quasifission processes, however the leading role in determining the outcome of the reaction is played by incompressibility, symmetry energy and the isoscalar coefficient of the surface term. This study unravels the complexity of the fusion and quasifission reaction dynamics and helps to understand the microscopic processes responsible for the final outcome of low energy heavy ion collisions in terms of relevant features of the nuclear effective interaction and associated equation of state (EoS).

I. INTRODUCTION

Understanding the dissipation mechanisms occurring in low energy heavy ion collisions represents one of the most challenging problems in nuclear reaction and structure studies [1–7]. Crucial information is provided by the investigation of strongly damped collisions of nuclei, that may lead to (incomplete) fusion, quasifission or deep-inelastic processes, looking at the degree of equilibration reached along the reaction path and at the features of the final reaction products [8–16]. In addition, in these reactions one can observe effects reflecting a delicate interplay between the microscopic single-particle dynamics and the possible occurrence of collective motion [9–11, 17, 18].

In particular, dissipative reaction dynamics plays an essential role in the synthesis of superheavy elements (SHE), a quite appealing challenge of modern nuclear physics [15, 19–26]. The synthesizing process, realized by fusing two heavy nuclei in the laboratory, can be schematically divided into three steps where both nuclear structure and dynamics are important: 1) the two nuclei find each other and their surfaces stick together; 2) the shape of the two nuclei evolves to form a compound nucleus; 3) the evaporation residue survives against statistical fission decay. These processes are usually related to the capture, compound nucleus formation and survival probabilities (see for instance [27, 28]) and two experimental methods, i.e., cold fusion with target nuclei close to the doubly magic nucleus ^{208}Pb and hot fusion with actinide target nuclei [15, 16], have been devised so far. It is rather clear that, apart from the occurrence of statistical

fission, the probability to form superheavy elements is strongly affected by the competition between compound nucleus formation and quasifission processes.

At low energies (close and/or above the Coulomb barrier), heavy ion reactions are governed, to a large extent, by one-body dissipation mechanisms (see for instance [29]). From a microscopic point of view, their description can be addressed within the Time Dependent Hartree Fock (TDHF) approach [12–16, 30–40], and its semi-classical approximation (the Vlasov equation) [8–11]. These mean-field approaches (including stochastic extensions, that account for quantum fluctuations) provide a suitable framework to study the many-body system at a fully microscopic level and have been successfully applied to describe fusion reactions, nucleon transfer and deep-inelastic collisions, as well as the quasifission dynamics [14, 39, 41–44]. Among possible examples, the prominent role of one-body dissipation is corroborated by the consistent results obtained, between TDHF and Vlasov calculations, in studies related to the Giant Dipole Resonance (GDR) and for charge asymmetric nuclear reactions just above the Coulomb barrier [9, 45], and by the excellent quantitative agreement between recent quasifission experimental results and model calculations which incorporate one-body dissipation and fluctuations [14]. In spite of the apparent simplicity of the reaction dynamics, quite intriguing features may manifest along the fusion/fission path, reflecting the complexity of the self-consistent mean-field. Indeed, apart from the expected sensitivity to the properties, such as charge, mass and deformation, of the two colliding nuclei, the reaction path is quite influenced also by the ingredients of the nuclear effective interaction employed in the calculations. It should be noticed that the latter is closely connected to the nuclear Equation of State (EoS), which plays an important role in nuclear structure [46, 47], dynamics of heavy ion

*Email address: zhengh@snnu.edu.cn

†Email address: colonna@lns.infn.it

collisions at intermediate energy [8–11, 48, 49] and astrophysical phenomena as well [50–52].

By considering collisions between either neutron poor or neutron rich systems, the impact of the isospin degree of freedom on the reaction dynamics has been explored in theoretical studies [8–16, 36–40]. Several investigations have also been devoted to the role of specific ingredients of the nuclear effective interaction. In particular, the influence of the symmetry energy, that is closely linked to the neutron-skin thickness, on the amplitude of the sub-barrier fusion cross section of neutron-rich nuclei has been evidenced in Ref. [53]. Other studies were dedicated to the sensitivity of isospin equilibration to the effective interaction, either in low-energy reactions, where collective pre-equilibrium dipole oscillations take place [9–11, 54–56], or for reactions at Fermi energies, where a sizable pre-equilibrium nucleon emission is observed [8, 51, 57, 58]. Reactions close to the Coulomb barrier, and more specifically at the frontier between fusion and other channels are also known to be sensitive to the spin orbit term [59–61] or the tensor interactions [62, 63].

In this paper, we aim at getting a deeper understanding of the interplay between fusion and quasifission processes in low energy heavy ion collisions. As stressed above, this is particularly important in the search of new SHE. In keeping with the spirit of previous studies [10, 53, 58], we investigate, within the TDHF approach, the impact of relevant ingredients of the nuclear effective interaction, such as incompressibility, symmetry energy, effective mass, Lane potential derivative, and surface terms, on the exit channel (fusion vs quasifission) of central heavy ion reactions close to the Coulomb barrier. Our goal is to establish possible connections between the reaction dynamics and global nuclear matter properties, in density regions around and below the saturation value. Such a comprehensive study is important to reach more reliable predictions about the probability to get compound nucleus formation. In turn, the comparison with available experimental data would allow one to extract information on specific aspects of the nuclear interaction, which are still poorly known.

The paper is organized as follows. In section II, we introduce the theoretical framework as well as the set of EoS employed in the calculations. In particular, we will consider EoS only differing by one ingredient, with respect to a reference case, to focus on the effect of that particular ingredient on the reaction process. In such a way, we can decouple the correlations among the different sectors of the EoS. In section III, we present the results obtained for selected reactions, discussing how the several EoS ingredients affect the exit channel. Conclusions and perspectives are drawn in section IV.

II. THEORETICAL FRAMEWORK AND EFFECTIVE INTERACTIONS

In the TDHF theory, the evolution of the one-body density matrix $\hat{\rho}(t)$ is determined by,

$$i\hbar\partial_t\hat{\rho}(t) = [h[\hat{\rho}], \hat{\rho}(t)], \quad (1)$$

where $h[\hat{\rho}] = \mathbf{p}^2/2m + U[\mathbf{p}, \rho]$ is the mean-field Hamiltonian with U as the self-consistent potential and $\rho(\mathbf{r})$ denoting the local density. Within the Density Functional Theory, the starting point is the energy density functional $\mathcal{E}[\rho]$, from which the corresponding nuclear EoS and the potential U can be consistently derived.

In the present work, we adopt Skyrme effective interactions, which are characterized in terms of nine interaction parameters ($t_0, t_1, t_2, t_3, x_0, x_1, x_2, x_3, \sigma$), plus the spin-orbit coupling constants $W_{0(i)}$ [64–67]. Apart from the spin-orbit term, the energy density is expressed in terms of the isoscalar, $\rho = \rho_n + \rho_p$, and isovector, $\rho_3 = \rho_n - \rho_p$, densities and kinetic energy densities ($\tau = \tau_n + \tau_p, \tau_3 = \tau_n - \tau_p$) as [9, 68–70]:

$$\begin{aligned} \mathcal{E}[\rho] &\equiv \mathcal{E}_{kin}(\tau) + \mathcal{E}_{pot}(\rho, \rho_3, \tau, \tau_3) \\ &= \frac{\hbar^2}{2m}\tau + C_0\rho^2 + D_0\rho_3^2 + C_3\rho^{\sigma+2} + D_3\rho^\sigma\rho_3^2 \\ &\quad + C_{eff}\rho\tau + D_{eff}\rho_3\tau_3 \\ &\quad + C_{surf}(\nabla\rho)^2 + D_{surf}(\nabla\rho_3)^2, \end{aligned} \quad (2)$$

where the coefficients $C_., D_.$ are combinations of the standard Skyrme parameters (see Appendix A). In particular, the terms with coefficients C_{eff} and D_{eff} are the momentum dependent contributions to the nuclear effective interaction. The Coulomb interaction is also considered in the calculations. It turns out to be useful to explicit the relations between the coefficients of the Skyrme interaction and relevant nuclear properties. In analogy with the studies of Refs. [71, 72], we will consider: saturation density ρ_0 ; energy per nucleon of symmetric nuclear matter at ρ_0 (E_0); incompressibility K_0 ; isoscalar effective mass m_s^* and isovector effective mass m_v^* at saturation density; symmetry energy at ρ_0 (J); slope of the symmetry energy at ρ_0 (L); strength of the isoscalar surface term $G_S = C_{surf}/2$ and strength of the isovector surface term $G_V = -D_{surf}/2$.

By this connection, it becomes straightforward to explore the impact of specific nuclear matter properties on the reaction dynamics. Here, instead of the isovector effective mass, we prefer to employ the derivative, with respect to the momentum p , of the Lane potential, which has a more intuitive physical meaning, related to the splitting of neutron and proton effective masses, m_n^* and m_p^* . Denoting by $U_i = \left. \frac{\partial \mathcal{E}_{pot}}{\partial \rho_i} \right|_p$ the single particle potential, where i stands for neutrons or protons and \mathcal{E}_{pot} is the potential part of the energy density functional,

Eq.(2), the Lane potential is written as

$$U_{Lane} = \frac{U_n - U_p}{2I} = 2D_0\rho + 2D_3\rho^{\sigma+1} + \frac{D_{eff}\tau_3}{I} + D_{eff}\rho\frac{p^2}{\hbar^2}, \quad (3)$$

where $I = \frac{\rho_n - \rho_p}{\rho}$ is the asymmetry parameter. Therefore, the Lane potential derivative reads:

$$\frac{dU_{Lane}}{dp} = \frac{2D_{eff}}{\hbar^2}\rho p = \left(\frac{1}{m_s^*} - \frac{1}{m_v^*}\right)p = \frac{f_I}{m}p, \quad (4)$$

where the parameter f_I has been introduced and m denotes the nucleon mass. f_I actually gives a measure of the neutron-proton effective mass splitting because the following relation holds: $\frac{1}{m_s^*} - \frac{1}{m_v^*} = \frac{1}{2I}\left(\frac{1}{m_n^*} - \frac{1}{m_p^*}\right)$ [58].

In our study, we will consider the recently introduced SAMi-J Skyrme effective interactions [73]. The corresponding parameters have been determined based on the SAMi fitting protocol [73]: binding energies and charge radii of some doubly magic nuclei, which allow the SAMi-J family to predict a reasonable saturation density, energy per nucleon and incompressibility modulus of symmetric nuclear matter; some selected spin-isospin sensitive Landau-Migdal parameters [74]; the neutron matter EoS of Ref. [75]. According to the strength of the momentum dependent terms, these interactions lead to an effective isoscalar nucleon mass $m_s^* = 0.675 m$ and a neutron-proton effective mass splitting $m_n^* - m_p^* = 0.023 mI$ MeV at saturation density, with the corresponding parameter $f_I = -0.0251$. This small mass splitting effect is associated with a quite flat momentum dependence of the symmetry potential. It should be noticed that the SAMi-J interactions exhibit a correlation between J and L , so that all interactions lead to the same value of the symmetry energy below normal density (at $\rho \approx 0.6\rho_0$), well describing the ground state properties of nuclei. For neutron-rich nuclei, the interactions with a larger L (and J) value predict a thicker neutron skin (see Tables I and II).

III. RESULTS AND DISCUSSIONS

We have performed TDHF calculations for the system $^{238}\text{U}+^{40}\text{Ca}$, at $E_{cm} = 203$ MeV and zero impact parameter. This reaction has been investigated in great detail, for a specified EoS and in the TDHF framework, in previous papers [37, 76], that we will consider as a reference for our study.

In practice, we use the EV8 code to initialize the two nuclei [77] and the TDHF-3D code developed in Refs. [30, 31, 43, 78] to follow the reaction dynamics. We adopt a 3D lattice mesh ($96 \times 40 \times 20$) with a mesh step of 0.8 fm, and a time step $\Delta t = 0.36$ fm/c. The initial distance between the two colliding nuclei is 26.4 fm.

The values of binding energy, neutron and proton root mean square radii and quadrupole deformation parameter are reported in Tables I and II, for the three SAMi-J interactions that we will consider in our analysis.

Interaction	$\sqrt{\langle r^2 \rangle_n}$	$\sqrt{\langle r^2 \rangle_p}$	neutron skin	β_2	BE/A (MeV)
SAMi-J27	3.360	3.410	-0.050	0.0	-8.210
SAMi-J31	3.357	3.405	-0.048	0.0	-8.374
SAMi-J35	3.350	3.396	-0.046	0.0	-8.507

TABLE I: Neutron and proton root mean square radii, and their difference, quadrupole deformation and binding energy for ^{40}Ca , as obtained with the SAMi-J interactions. The experimental value of the binding energy is BE/A=-8.551 MeV [79, 80].

Interaction	$\sqrt{\langle r^2 \rangle_n}$	$\sqrt{\langle r^2 \rangle_p}$	neutron skin	β_2	BE/A (MeV)
SAMi-J27	5.927	5.802	0.125	0.251	-7.547
SAMi-J31	6.02	5.81	0.21	0.228	-7.524
SAMi-J35	6.10	5.815	0.285	0.228	-7.499

TABLE II: Neutron and proton root mean square radii, and their difference, quadrupole deformation and binding energy for ^{238}U , as obtained with the SAMi-J interactions. The experimental value for the binding energy is BE/A=-7.570 MeV [79, 80].

The beam energy considered is in the range of the transition from fusion to quasifission processes, thus it is well adapted to our study of the competition between the two reaction mechanisms. It should be noticed that ^{40}Ca is spherical and this will reduce the number of collision configurations and the complexity of the calculations [39, 40]. On the other hand, since the ground state of ^{238}U is deformed, it is worthwhile to consider reaction configurations corresponding to two possible projectile-target orientations: side and tip. For the tip orientation, at the energy considered, quasifission is always observed in TDHF calculations [37–39]. We will show just one tip collision case, as an example, and then concentrate on side collisions in our study. The trajectory of the reaction is traced by evaluating the quadrupole moment $Q_2(t) = \langle 2x^2 - y^2 - z^2 \rangle$ of the composite system, with x denoting the beam axis. An increasing trend of $Q_2(t)$ indicates that the system is evolving towards quasifission. On the other hand, if $Q_2(t)$ stays around a constant value, then the system fuses. To check the outcome of the reaction, one can also look directly at density contour plots at different time instants, as shown in Fig. 1 for the tip collision of the reaction considered, with the effective interaction SAMi-J31. One can see that the quasifission happens in a few zs which is consistent with the statements in Refs. [37–39].

Let us now turn to discuss side collisions. In Fig. 2, the time evolution of the quadrupole moment of the com-

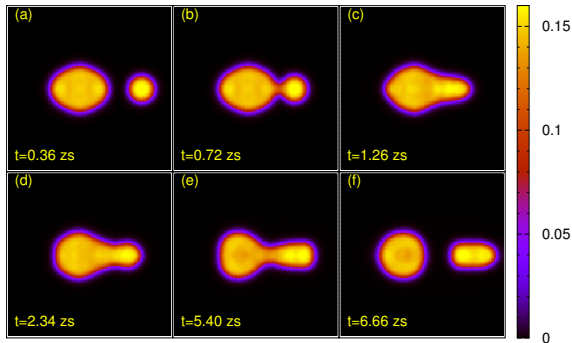


FIG. 1: (Color online) Density contour plot at different time instants for the tip collision of the reaction $^{238}\text{U}+^{40}\text{Ca}$ (tip orientation) at $E_{cm} = 203$ MeV and $b=0$ fm. The SAMi-J31 interaction is employed.

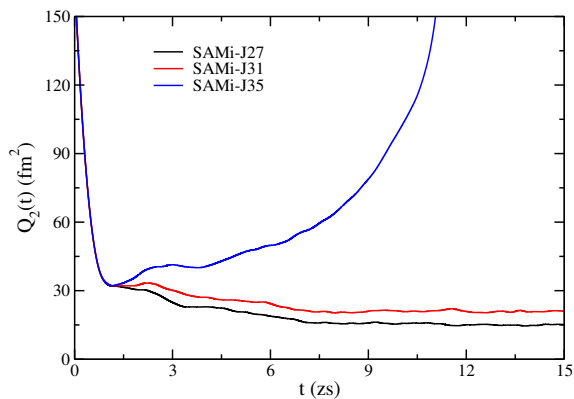


FIG. 2: (Color online) The quadrupole moment time evolution of the reaction $^{238}\text{U}+^{40}\text{Ca}$ (side orientation) at $E_{cm} = 203$ MeV and $b=0$ fm, for three SAMi-J EoS.

posite system is shown for calculations corresponding to three different SAMi-J interactions, namely SAMi-J27, SAMi-J31 and SAMi-J35, whose label denotes the symmetry energy value (J) at saturation density. Clearly, we can see that the SAMi-J35 parametrization leads to quasifission, whereas the other two SAMi-J EoS are associated with fusion. Corresponding density contour plots are shown in Figs. 3 and 4 for SAMi-J31 and SAMi-J35, respectively, in order to better display this dual behavior. The competition between fusion and quasifission has been interpreted in terms of the features exhibited by the fusion barrier, V_B , as evaluated within the Density Constrained - TDHF method [16, 40, 76], when employing different effective interactions. The results shown on Fig. 2 would indicate that a larger symmetry energy slope, which results in a thicker neutron skin for neutron rich nuclei, makes the reaction system easier to separate. However, as we will discuss in the following, the three parameterizations also differ by other aspects.

To extend our discussion about the sensitivity of the reaction path to the ingredients of the effective inter-

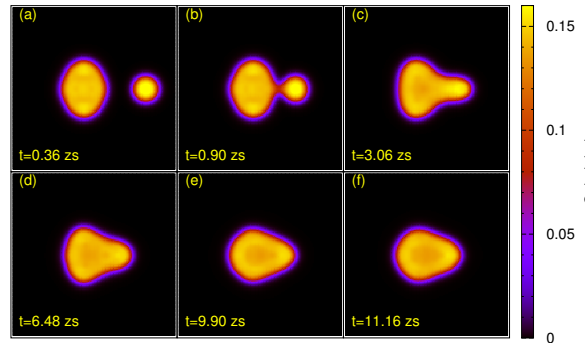


FIG. 3: (Color on line) Same as in Fig. 1, but for the side collision.

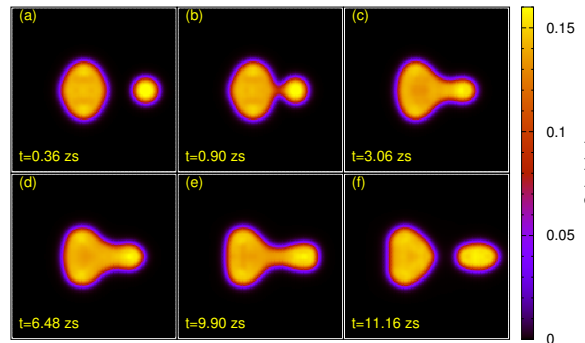


FIG. 4: (Color online) Same as in Fig. 1, but for the side collision, with SAMi-J35.

action, we will enlarge the set of Skyrme interactions employed in the TDHF calculations. In addition to the three SAMi-J parametrizations, we will consider interactions corresponding to the variations of six quantities, with respect to the SAMi-J31, that is taken as a reference: the symmetry energy slope L (keeping the $J - L$ correlation discussed above), the incompressibility, the effective mass, the parameter f_I and the surface terms G_S and G_V . ρ_0 and E_0 are adopted from SAMi-J31 for all the EoS. We have checked that the binding energy and the root mean square of proton and neutron radii of ^{238}U and ^{40}Ca are well preserved (within a few percent) under those operations, with the neutron skin thickness of ^{238}U being mainly determined by the symmetry energy slope L . For the convenience of description, we list the properties of the different EoS in Table III. The EoS name follows the convention that we only label the terms which are different, with respect to the ingredients of the SAMi-J31 parametrization.

No	EoS	ρ_0 (fm $^{-3}$)	E_0 (MeV)	K_0 (MeV)	J (MeV)	L (MeV)	m_s^*/m	m_v^*/m	f_I	G_S	G_V	Result
	SAMi-J27	0.160	-15.93	245	27	30	0.675	0.664	-0.0251	149.2	-8.6	Fusion
S1	SAMi-J31	0.156	-15.83	245	31	74	0.675	0.664	-0.0251	140.9	3.1	Fusion
	SAMi-J35	0.154	-15.69	245	35	115	0.675	0.664	-0.0251	131.1	15.4	Fission
S2	J27	0.156	-15.83	245	27	30	0.675	0.664	-0.0251	140.9	3.1	Fusion
S3	J35	0.156	-15.83	245	35	115	0.675	0.664	-0.0251	140.9	3.1	Fusion
	Gs35	0.156	-15.83	245	31	74	0.675	0.664	-0.0251	131.1	3.1	Fission
	J35_Gs35	0.156	-15.83	245	35	115	0.675	0.664	-0.0251	131.1	3.1	Fission
	J35_Gv35	0.156	-15.83	245	35	115	0.675	0.664	-0.0251	140.9	15.4	Fusion
	J35_Gs35Gv35	0.156	-15.83	245	35	115	0.675	0.664	-0.0251	131.1	15.4	Fission
S4	K200	0.156	-15.83	200	31	74	0.675	0.664	-0.0251	140.9	3.1	Fission
S5	K290	0.156	-15.83	290	31	74	0.675	0.664	-0.0251	140.9	3.1	Fusion
S6	ms085	0.156	-15.83	245	31	74	0.85	0.832	-0.0251	140.9	3.1	Fusion
S7	ms100	0.156	-15.83	245	31	74	1.0	0.976	-0.0251	140.9	3.1	Fusion
	Gs35_ms085	0.156	-15.83	245	31	74	0.85	0.832	-0.0251	131.1	3.1	Fusion
	Gs35_ms100	0.156	-15.83	245	31	74	1.0	0.976	-0.0251	131.1	3.1	Fusion
S8	fl020	0.156	-15.83	245	31	74	0.675	0.781	0.20	140.9	3.1	Fusion
S9	fln024	0.156	-15.83	245	31	74	0.675	0.581	-0.24	140.9	3.1	Fusion
	Gs35_fl020	0.156	-15.83	245	31	74	0.675	0.781	0.2	131.1	3.1	Fission
	Gs35_fln024	0.156	-15.83	245	31	74	0.675	0.581	-0.24	131.1	3.1	Fission

TABLE III: The properties of the different EoS considered in the present work, and the exit channel of the reaction. The units of G_S and G_V are MeV·fm 5 . Associated values of standard Skyrme parameters (t_i, x_i) are given in Appendix A.

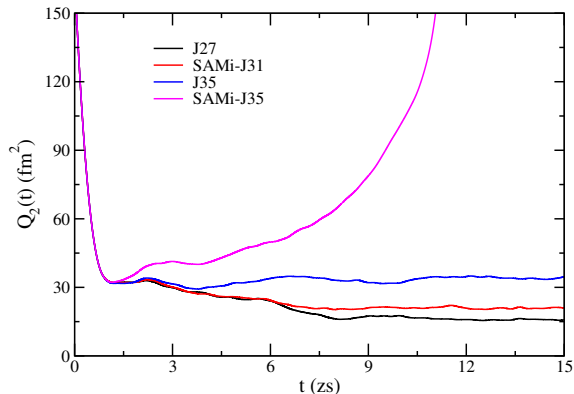


FIG. 5: (Color online) The symmetry energy dependence of the quadrupole moment evolution of the reaction considered (same as in Fig. 2). All reactions are performed at $E_{cm} = 203$ MeV and $b=0$ fm.

A. Symmetry energy effects

In Fig. 5, we show the quadrupole moment evolution of the reaction considered, for calculations employing the EoS obtained by varying the symmetry energy properties (S1, S2 and S3). One can notice that the result differs from what is shown in Fig. 2, where the three SAMi-J parametrizations are compared. Indeed SAMi-J35 calculations (also reported in Fig. 5) lead to quasi-fission, where the S3 parametrization does not, though it

presents the same symmetry energy features. This can be explained by considering that the three SAMi-J EoS are characterized not only by a different (J - L) combination, but also exhibit different surface properties, see Table III.

However, one observes that the quadrupole moment associated with the EoS considered here is ordered by the symmetry energy, i.e., the larger the symmetry energy, the larger the quadrupole moment. Owing to the neutron excess in our system, a larger symmetry energy around normal density leads to a more repulsive dynamics, as one would intuitively expect. However, for the interactions considered, the quadrupole moment keeps quite smaller than the result associated with the SAMi-J35. This indicates that surface terms may play a very important role in the reaction dynamics, as we will discuss in the following section.

B. Surface term effects

In Fig. 6, we show the time evolution of the quadrupole moment Q_2 , as obtained for the EoS corresponding to different surface term (G_S and G_V) combinations, as indicated in Table III. As it is shown in panel (a), by comparing the results associated with SAMi-J31 and Gs35, a reduced G_S surface term helps the system to separate, even in the case of a parametrization having the same symmetry energy as SAMi-J31, that is not repulsive enough to lead to quasifission (see Fig. 5). Com-

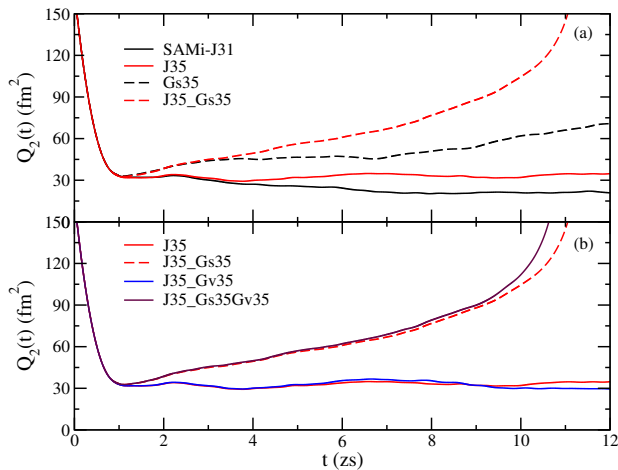


FIG. 6: (Color online) Surface effects on the quadrupole moment evolution of the reaction considered (same as in Fig. 2). All reactions are performed at $E_{cm} = 203$ MeV and $b=0$ fm.

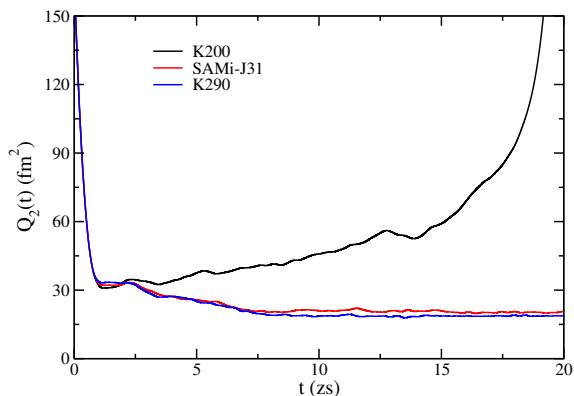


FIG. 7: (Color online) The incompressibility dependence of the quadrupole moment evolution, for the same reaction as in Fig. 2. All reactions are performed at $E_{cm} = 203$ MeV and $b=0$ fm.

combined with a larger symmetry energy (J35), the surface term reduction leads to a quite fast quasifission dynamics (J35_Gs35). This result can be explained considering that, along the approaching phase a reduced surface term favors the formation of more elongated configurations, helping fission. On the other hand, by considering interactions where also G_V is changed significantly (see Table III), panel (b) shows that the isovector surface term has only a tiny effect on the reaction dynamics.

C. Effects of the incompressibility K_0

In Fig. 7, we show the results corresponding to three EoS with different incompressibilities (S1, S4, S5). For $K_0=200$ MeV the system gets quasifission, whereas fusion is observed for the other two larger K_0 values. The observed dependence of our results on the incompressibility is related to the fact that it is more difficult to com-

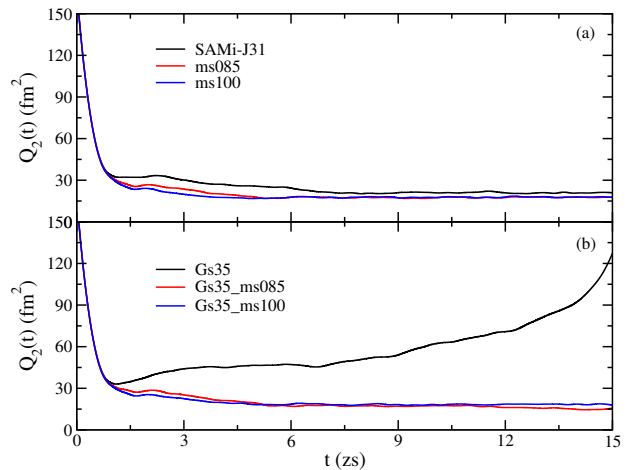


FIG. 8: (Color online) The dependence of the quadrupole moment evolution on the isoscalar effective mass. Same reaction system as in Fig. 2. All reactions are performed at $E_{cm} = 203$ MeV and $b=0$ fm.

press or to expand the composite reaction system formed along the reaction path, if K_0 is large. Indeed, in this case, the system needs to pay more energy to undergo density oscillations of a given amplitude, as compared to the calculations corresponding to smaller K_0 values. We observe that, at the compression stage, the system exhibits the smallest quadrupole moment for the case $K_0=200$ MeV, because the system is easier to compress and becomes more compact. Then, along the expansion phase, the quadrupole moment increases significantly because it is easier to expand the system towards densities below the saturation value. When the deformed system overcomes a given threshold, the reaction path will result in quasifission. Apparently, this does not happen for the cases corresponding to $K_0=245$ MeV (SAMi-J31) and $K_0=290$ MeV (S5), for which fusion is finally observed and the quadrupole moment oscillates around a constant value. Clearly, density oscillations of larger amplitude help the system to fission.

D. Effects of the isoscalar effective mass m_s^*

The effect of the isoscalar effective mass on the quadrupole moment evolution of the reaction considered is shown in Fig. 8, by considering parametrizations with larger effective mass than the value associated with SAMi-J31 (S6, S7). One can see that, starting from a situation where fusion is observed (SAMi-J31), the increase of the nucleon effective mass does not change the reaction dynamics; however the calculations corresponding to larger effective mass values lead to more compact configurations, associated with a smaller quadrupole moment. In Fig. 8(b), we explore the impact of the isoscalar effective mass also on a trajectory leading to quasifission (corresponding to the parametrization Gs35). In this

case, it is observed that a larger effective mass changes the reaction dynamics, leading to fusion. In the latter case, the quadrupole evolution exhibits the same pattern in panels (a) and (b). To understand these results, one may consider that particles having a smaller effective mass can move faster in the nuclear potential, so that for the system it is easier to escape from the attractive nuclear interaction and evolve towards quasifission. This is in line with what is observed in the study of collective modes (such as the GDR), where effective interactions with small effective mass lead to higher oscillation frequency and to a more abundant particle emission [9]. One can also argue that particles with a small isoscalar effective mass can invert more easily their direction of motion, helping the system expansion. On the other hand, a larger effective mass favors the trapping of the system into the nuclear potential, leading to fusion. A careful inspection of Fig. 8(b) reveals that, at the early stage, the quadrupole moment is larger in the case of the interaction with isoscalar effective mass equal to $0.85m$, with respect to the ‘ms100’ case ($m_s = m$), but this trend is inverted at a later stage. This can be attributed to the fact that momentum dependent interactions, lead to a larger (smaller) repulsion for nucleons with momenta larger (smaller) than the Fermi momentum, with respect to the ‘ms100’ case.

Thus, once the system overcomes the fusion barrier, more compact configurations are observed in the ‘ms085’ case, indicating a larger attraction at small momenta.

E. Effects of f_I

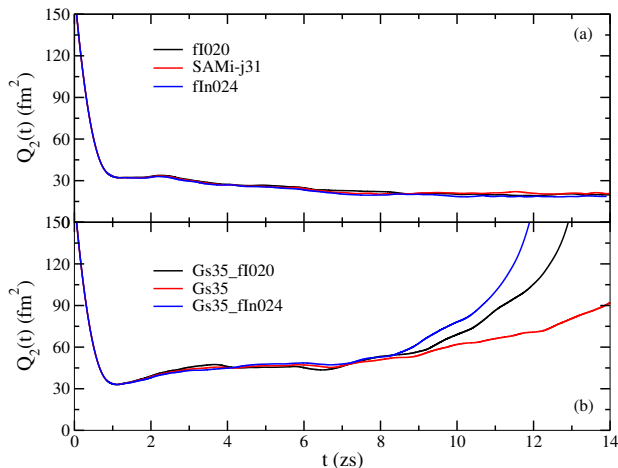


FIG. 9: (Color online) The f_I dependence of the quadrupole moment evolution of the system considered (same as in Fig. 2). All reactions are performed at $E_{cm} = 203$ MeV and $b=0$ fm.

We now concentrate on the reaction dynamics associated with the three EoS having different values of f_I , adopting the isoscalar surface term of SAMi-J31 (S1, S8,

S9), see Fig. 9(a), and of SAMi-J35, see Fig. 9(b). One can observe that the system ends up with fusion for the three cases in panel (a) and quasifissions for the three cases in panel (b). Thus the f_I parameter does not affect crucially the outcome of the reaction, either fusion or quasifission. The ordering observed in panel (b) may result from a delicate balance between symmetry energy, n/p effective mass splitting and Coulomb repulsion effects. Increasing the neutron-proton effective mass splitting, with $m_n^* < m_p^*$ (‘fI020’ case), leads to a larger neutron repulsion, in addition to symmetry energy effects. As a result, we observe a faster quasifission dynamics. On the other hand, a n/p effective splitting of opposite sign, with $m_p^* < m_n^*$ (‘fIn024’ case), tends to counterbalance symmetry energy effects. However, in this situation, the relative role of the Coulomb repulsion is enhanced, that may also lead to a faster dynamics, as we actually observe in Fig. 9(b). It may be interesting to note that similar effects of the neutron/proton effective mass splitting are discussed for observables typical of nuclear reactions in the Fermi energy domain, such as the isotopic content of the pre-equilibrium nucleon emission [58].

IV. CONCLUSIONS

To summarize, we have investigated, by employing a variety of effective interactions within the TDHF approach, the impact of several EoS ingredients on the exit channel (fusion vs quasifission) of nuclear reactions at energies close to the Coulomb barrier. In particular, we build up explicit relations between the coefficients of the Skyrme interaction and relevant nuclear properties, such as incompressibility, symmetry energy, effective mass, Lane potential derivative and surface terms, in some analogy with the studies of Refs. [71, 72]. We consider EoS mainly differing by one ingredient, with respect to a reference case, to focus on the effect of that particular ingredient on the reaction process. In such a way, we are able to decouple possible correlations among the different sectors of the EoS. The trajectory of the reaction is traced by evaluating the quadrupole moment $Q_2(t)$ of the composite system or by looking at the density contour plots. Calculations are shown for the reaction $^{238}\text{U} + ^{40}\text{Ca}$ at $E_{cm} = 203$ MeV and zero impact parameter. We observe that all the ingredients listed above contribute to the competition between fusion and quasifission processes, however the leading role in determining the outcome of the reaction is played by incompressibility, symmetry energy and the isoscalar coefficient of the surface term. These results enable us to establish possible connections between the reaction dynamics and global nuclear matter properties, opening the perspective to learn on specific aspects which are still poorly known. We also note that, when quasifission is observed, the features of the two final fragments may depend on the effective interaction considered, also in connection with the contact time between the two interacting nu-

No	EoS	t_0	t_1	t_2	t_3	x_0	x_1	x_2	x_3	σ
	SAMi-J27	-1876.09	481.087	-75.7069	10184.6	0.482235	-0.557967	0.213066	1.00219	0.254634
S1	SAMi-J31	-1844.28	460.727	-110.200	10112.4	-0.0237088	-0.458608	-0.431251	0.00764843	0.268372
	SAMi-J35	-1799.53	436.229	-144.972	9955.45	-0.443908	-0.343557	-0.783861	-0.882427	0.284323
S2	J27	-1844.27	460.727	-110.200	10112.4	0.478794	-0.458608	-0.431252	1.012559	0.268374
S3	J35	-1844.27	460.727	-110.200	10112.4	-0.461008	-0.458608	-0.431252	-0.879839	0.268374
	Gs35	-1844.28	434.803	-84.2766	10112.4	-0.0237087	-0.456140	-0.410106	0.00764882	0.268374
	J35_Gs35	-1844.27	434.803	-84.2767	10112.4	-0.461008	-0.456140	-0.410106	-0.879839	0.268374
	J35_Gv35	-1844.27	460.727	-175.617	10112.4	-0.461008	-0.352118	-0.736234	-0.879839	0.268374
	J35_Gs35Gv35	-1844.27	434.803	-149.694	10112.4	-0.461008	-0.343301	-0.777144	-0.879839	0.268374
S4	K200	5698.04	460.727	-110.200	-36164.8	0.0177978	-0.458608	-0.431251	0.00764843	-0.0421665
S5	K290	-1295.07	460.727	-110.200	8342.72	-0.0370067	-0.458608	-0.431251	0.00764843	0.578726
S6	ms085	-1696.12	406.841	-271.859	11451.3	-0.105374	-0.453125	-0.472133	-0.281046	0.354121
S7	ms100	-1654.78	375.621	-365.519	12510.9	-0.130771	-0.449229	-0.479273	-0.397744	0.388782
	Gs35_ms085	-1696.12	380.917	-245.935	11451.3	-0.105374	-0.449935	-0.469195	-0.281046	0.354121
	Gs35_ms100	-1654.78	349.697	-339.596	12511.0	-0.130771	-0.445466	-0.477691	-0.397744	0.388782
S8	fl020	-1844.27	460.727	-349.145	10112.4	0.144457	-0.588264	-0.991579	0.514540	0.268374
S9	fln024	-1844.27	460.727	117.911	10112.4	-0.184250	-0.334830	-2.015208	-0.476261	0.268374
	Gs35_fl020	-1844.27	434.803	-323.221	10112.4	0.144457	-0.593527	-1.031006	0.514540	0.268374
	Gs35_fln024	-1844.27	434.803	143.834	10112.4	-0.184250	-0.324982	-1.742118	-0.476261	0.268374

TABLE IV: The standard parameters of the Skyrme interactions listed in Table III.

clei. Results concerning the corresponding charge/mass and energy sharing will be the object of a forthcoming publication. We finally stress that a deeper understanding of the interplay between fusion and quasifission processes in low energy heavy-ion collisions is instrumental for the search of new SHE in the laboratory.

V. ACKNOWLEDGMENTS

This project has received funding from the European Union's Horizon 2020 research and innovation programme under grant agreement N. 654002.

Appendix A

The relations between the $C_{..}$ and $D_{..}$ coefficients of the energy density functional of Eq.(2) and the standard parameters of the Skyrme interactions are given below:

$$C_0 = \frac{3}{8}t_0, \quad (\text{A1})$$

$$D_0 = -\frac{1}{8}t_0(2x_0 + 1), \quad (\text{A2})$$

$$C_3 = \frac{1}{16}t_3, \quad (\text{A3})$$

$$D_3 = -\frac{1}{48}t_3(2x_3 + 1), \quad (\text{A4})$$

$$C_{eff} = \frac{1}{16}[3t_1 + t_2(4x_2 + 5)], \quad (\text{A5})$$

$$D_{eff} = -\frac{1}{16}[t_1(2x_1 + 1) - t_2(2x_2 + 1)], \quad (\text{A6})$$

$$C_{surf} = \frac{1}{64}[9t_1 - t_2(4x_2 + 5)], \quad (\text{A7})$$

$$D_{surf} = -\frac{1}{64}[3t_1(2x_1 + 1) + t_2(2x_2 + 1)]. \quad (\text{A8})$$

From the $C_{..}$, $D_{..}$ coefficients of Eq.(2), the Lane potential Eq. (3) and its derivative Eq. (4) can be evaluated. In Table IV we list the parameters of the Skyrme interactions employed in our study, in their standard form. In analogy with the studies of Refs. [71, 72], the standard Skyrme parameters are derived imposing to reproduce nuclear matter properties and surface effects (see Section II). For the spin-orbit term, the coefficients corresponding to the SAMi-J interactions are adopted for all the interactions considered in our study: $W_{01} = 216.874$ and $W_{02} = -133.570$.

-
- [1] W. U. Schröder and J. R. Huizenga, *Treatise on Heavy-Ion Science*, edited by D. A. Bromley (Plenum, New York, 1984).
- [2] H. Feldmeier, Rep. Prog. Phys. **50**, 915 (1987).
- [3] D. Lacroix, S. Ayik, and P. Chomaz, Prog. Part. Nucl. Phys. **52**, 497 (2004).
- [4] C. Simenel, B. Avez, and D. Lacroix, Quantum Many-Body Dynamics: Applications to Nuclear Reactions (VDM Verlag, Sarrebruck, 2010).
- [5] D. Lacroix and S. Ayik, Eur. Phys. J. A **50**, 95 (2014).
- [6] D. Lacroix, Y. Tanimura, G. Scamps and C. Simenel, Int. J. Mod. Phys. E **24**, 1541005 (2015).
- [7] T. Nakatsukasa, K. Matsuyanagi, M. Matsuo, and K. Yabana, Rev. Mod. Phys. **88**, 045004 (2016).
- [8] V. Baran, M. Colonna, V. Greco and M. Di Toro, Phys. Rept. **410**, 335 (2005).
- [9] H. Zheng, S. Burrello, M. Colonna and V. Baran, Phys. Lett. B **769**, 424 (2017).
- [10] H. Zheng, S. Burrello, M. Colonna and V. Baran, Phys. Rev. C **94**, 014313 (2016).
- [11] C. Rizzo, V. Baran, M. Colonna, A. Corsi and M. Di Toro, Phys. Rev. C **83**, 014604 (2011).
- [12] Y. Tanimura, D. Lacroix and S. Ayik, Phys. Rev. Lett. **118**, 152501 (2017).
- [13] Y. Tanimura, D. Lacroix and G. Scamps, Phys. Rev. C **92**, 034601 (2015).
- [14] E. Williams *et al.*, Phys. Rev. Lett. **120**, 022501 (2018).
- [15] D. J. Hinde *et al.*, Phys. Rev. C **97**, 024616 (2018).
- [16] A. S. Umar, V. E. Oberacker and C. Simenel, Phys. Rev. C **94**, 024605 (2016).
- [17] D. Savran, T. Aumann and A. Zilges, Prog. Part. Nucl. Phys. **70**, 210 (2013).
- [18] C. Simenel, Ph. Chomaz, and G. de France, Phys. Rev. C **76**, 024609 (2007).
- [19] Y. A. Lazarev *et al.*, Phys. Rev. Lett. **75**, 1903 (1995).
- [20] Y. T. Oganessian *et al.*, Phys. Rev. Lett. **83**, 3154 (1999).
- [21] Y. T. Oganessian *et al.*, Phys. Rev. Lett. **104**, 142502 (2010).
- [22] Y. T. Oganessian *et al.*, Phys. Rev. Lett. **108**, 022502 (2012).
- [23] Y. T. Oganessian *et al.*, Phys. Rev. Lett. **109**, 162501 (2012).
- [24] Y. T. Oganessian and V. K. Utyonkov, Nucl. Phys. A **944**, 62 (2015).
- [25] J. Khuyagbaatar *et al.*, Phys. Rev. Lett. **112**, 172501 (2014).
- [26] J. Khuyagbaatar *et al.*, Phys. Rev. Lett. **115**, 242502 (2015).
- [27] G. G. Adamian, N. V. Antonenko, S. P. Ivanova, and W. Scheid, Phys. Rev. C **62**, 064303 (2000).
- [28] G. G. Adamian, N. V. Antonenko, and W. Scheid, Phys. Rev. C **69**, 014607 (2004).
- [29] P. Fröbrich and R. Lipperheide, *Theory of Nuclear Reactions* (Oxford University Press, New York, 1996).
- [30] D. Lacroix, arXiv:nucl-th/0202063.
- [31] K. Washiyama and D. Lacroix, Phys. Rev. C **78**, 024610 (2008).
- [32] S. Ayik, K. Washiyama, and D. Lacroix, Phys. Rev. C **79**, 054606 (2009).
- [33] K. Washiyama, S. Ayik, and D. Lacroix, Phys. Rev. C **80**, 031602(R) (2009).
- [34] B. Yilmaz, S. Ayik, D. Lacroix, and K. Washiyama, Phys. Rev. C **83**, 064615 (2011).
- [35] B. Yilmaz, S. Ayik, D. Lacroix, and O. Yilmaz, Phys. Rev. C **90**, 024613 (2014).
- [36] K. Vo-Phuoc, C. Simenel and E. C. Simpson, Phys. Rev. C **94**, 024612 (2016).
- [37] V. E. Oberacker, A. S. Umar and C. Simenel, Phys. Rev. C **90**, 054605 (2014).
- [38] C. Simenel, Eur. Phys. J. A **48**, 152 (2012).
- [39] A. Wakhle *et al.*, Phys. Rev. Lett. **113**, 182502 (2014).
- [40] A. S. Umar, V. E. Oberacker, J. A. Maruhn and P.-G. Reinhard, Phys. Rev. C **81**, 064607 (2010).
- [41] C. Simenel, Phys. Rev. Lett. **105**, 192701 (2010).
- [42] C. Simenel, Phys. Rev. Lett. **106**, 112502 (2011).
- [43] G. Scamps and D. Lacroix, Phys. Rev. C **87**, 014605 (2013).
- [44] K. Sekizawa and K. Yabana, Phys. Rev. C **88**, 014614 (2013) Erratum: [Phys. Rev. C **93**, 029902 (2016)].
- [45] S. Burrello, H. Zheng, M. Colonna, D. Lacroix, X. Roca-Maza and G. Scamps, in preparing.
- [46] G. Scamps and D. Lacroix, Phys. Rev. C **88**, 044310 (2013).
- [47] G. Scamps and D. Lacroix, Phys. Rev. C **89**, 034314 (2014).
- [48] P. Chomaz, M. Colonna and J. Randrup, Phys. Rept. **389**, 263 (2004).
- [49] A. Bonasera, F. Gulminelli and J. Molitoris, Phys. Rept. **243**, 1 (1994).
- [50] G. Giuliani, H. Zheng and A. Bonasera, Prog. Part. Nucl. Phys. **76**, 116 (2014).
- [51] B. A. Li, L. W. Chen and C. M. Ko, Phys. Rept. **464**, 113 (2008).
- [52] J. M. Lattimer and M. Prakash, Phys. Rept. **442**, 109 (2007).
- [53] P.-G. Reinhard, A. S. Umar, P. D. Stevenson, J. Piekarewicz, V. E. Oberacker and J. A. Maruhn, Phys. Rev. C **93**, 044618 (2016).
- [54] V. Baran, D.M. Brink, M. Colonna and M. Di Toro, Phys. Rev. Lett. **87**, 182501 (2001).
- [55] D. Pierrotsakou *et al.*, Phys. Rev. C **80**, 024612 (2009).
- [56] V. Baran, M. Cabibbo, M. Colonna, M. Di Toro and N. Tsoneva, Nucl. Phys. A **679**, 373 (2001).
- [57] V. Baran, M. Colonna, M. Di Toro *et al.* Phys. Rev. C **72**, 064620 (2005).
- [58] Y. Zhang, M. B. Tsang and Z. Li, Phys. Lett. B **749**, 262 (2015).
- [59] A. S. Umar, M. R. Strayer, and P. G. Reinhard, Phys. Rev. Lett. **56**, 2793 (1986).
- [60] J. A. Maruhn, P.-G. Reinhard, P. D. Stevenson, and M. R. Strayer, Phys. Rev. C **74**, 027601 (2006).
- [61] G.-F. Dai, L. Guo, E.-G. Zhao, and S.-G. Zhou, Phys. Rev. C **90**, 044609 (2014).
- [62] P. D. Stevenson, E. B. Suckling, S. Fracasso, M. C. Barton, and A. S. Umar, Phys. Rev. C **93**, 054617 (2016).
- [63] Lu Guo, Cédric Simenel, Long Shi and Chong Yu, Phys. Lett. B **782**, 401 (2018).
- [64] T.H.R. Skyrme, Philos. Mag. **1**, 1043 (1956); Nucl. Phys. **9**, 615 (1959); *ibid.* **9**, 635 (1959).
- [65] D. Vautherin and D. M. Brink, Phys. Rev. C **5**, 626 (1972).
- [66] M. Bender, P.H. Heenen and P.G. Reinhard, Rev. Mod.

- Phys. **75**, 121 (2003).
- [67] J. R. Stone and P.-G. Reinhard, Prog. Part. Nucl. Phys. **58**, 587 (2007).
- [68] Ad.R. Raduta *et al.*, Eur. Phys. J. A **50**, 24 (2014).
- [69] E. Lipparini and S. Stringari, Phys. Rep. **175**, 103 (1989).
- [70] T. Lesinski, K. Bennaceur, T. Duguet and J. Meyer, Phys. Rev. C **74**, 044315 (2006).
- [71] L. W. Chen, B. J. Cai, C. M. Ko, B. A. Li, C. Shen and J. Xu, Phys. Rev. C **80**, 014322 (2009).
- [72] L. W. Chen, C. M. Ko, B. A. Li and J. Xu, Phys. Rev. C **82**, 024321 (2010).
- [73] X. Roca-Maza, G. Colò, H. Sagawa, Phys. Rev. C **86**, 031306(R) (2012); X. Roca-Maza *et al.*, *ibid.* **87**, 034301 (2013).
- [74] L.G. Cao, G. Colò, and H. Sagawa, Phys. Rev. C **81**, 044302 (2010).
- [75] R.B. Wiringa, V. Fiks, and A. Fabrocini, Phys. Rev. C **38**, 1010 (1988).
- [76] A. S. Umar, V. E. Oberacker and C. Simenel, Phys. Rev. C **92**, 024621 (2015).
- [77] P. Bonche, H. Flocard, and P.-H. Heenen, Comput. Phys. Commun. **171**, 49 (2005).
- [78] K.-H. Kim, T. Otsuka, and P. Bonche, J. Phys. G **23**, 1267 (1997).
- [79] H. De Vries, C. W. De Jager and C. De Verries, At. Data Nucl. Data Tables **36**, 495 (1987); G. Audi and A. H. Wapstra, Nucl. Phys. A **595**, 409 (1995); I. Angeli and K. P. Marinova, At. Data Nucl. Data Tables **99**, 69 (2013).
- [80] <https://www.nndc.bnl.gov>.